






Investigating the $4D_{3/2}|3, \pm 2\rangle \rightarrow 4D_{5/2}|3, \pm 2\rangle$ transition in Nb^{4+} for a THz atomic clockJyoti ¹, A. Chakraborty ^{2,3}, Zhiyang Wang,¹ Jia Zhang ¹, Jingbiao Chen,^{1,4,*} Bindhya Arora ^{5,6} and B. K. Sahoo ^{2,†}¹*Institute of Quantum Electronics, School of Electronics, Peking University, Beijing 100871, People's Republic of China*²*Atomic, Molecular and Optical Physics Division, Physical Research Laboratory, Navrangpura, Ahmedabad 380009, India*³*Indian Institute of Technology Gandhinagar, Palaj, Gandhinagar 382355, India*⁴*Hefei National Laboratory, Hefei 230088, People's Republic of China*⁵*Department of Physics, Guru Nanak Dev University, Amritsar, Punjab 143005, India*⁶*Perimeter Institute for Theoretical Physics, Waterloo, Ontario, Canada N2L 2Y5*

(Received 16 September 2024; revised 10 December 2024; accepted 10 February 2025; published 21 February 2025)

In this work, the $4D_{3/2}|3, \pm 2\rangle \rightarrow 4D_{5/2}|3, \pm 2\rangle$ transition in the Nb^{4+} ion is identified as a promising candidate for a terahertz (THz) atomic clock, with the transition frequency occurring at 56.0224 THz. This transition is primarily driven by the magnetic dipole decay channel, which can easily be accessed by a laser. We focus on the stable ^{93}Nb isotope, which has 100% natural abundance and a nuclear spin of $I = 9/2$ for experimental advantage. Our data analysis allows us to estimate potential systematic shifts in the proposed clock system, including those due to blackbody radiation, electric quadrupole, second-order Zeeman, and second-order Doppler shifts. The scheme presented in this study can help suppress the ac Stark and electric quadrupole shifts in the clock-frequency measurement. All these analyses suggest that the proposed THz atomic clock using Nb^{4+} could be valuable in both quantum thermometry and frequency metrology.

DOI: [10.1103/PhysRevA.111.022813](https://doi.org/10.1103/PhysRevA.111.022813)

I. INTRODUCTION

Atomic clocks are often used as the timekeeping devices which define the international standard of time. Recent technological advancement in atomic physics has improved the precision of these atomic clocks to an extent that these devices lose only a second over several billion years. Atomic clocks were recently used in the investigation of various phenomena of fundamental physics, including the search for dark matter [1], the variation of fundamental physical constants [2], relativistic geodesy [3,4], gravitational-wave detection [5–7], and the description of interactions beyond the standard-model particle physics [8]. Most existing atomic clocks operate in both optical and microwave ranges, but lately, the operating range of these devices has been expanded to the terahertz (THz) range based on the application of various ingenious modes of THz electromagnetic radiation in sensing, spectroscopy, and communication [9] and for the analysis of interstellar matter [10].

THz clock transitions are high-frequency transitions of the order of 10^{12} Hz; hence, are proved to be highly sensitive to blackbody radiation (BBR) and can be used in quantum thermometers, especially in remote-sensing satellites [11]. Moreover, the THz-frequency standard also has applications in next-generation navigation, communication and sensing systems [12], and commercial THz instruments such as detectors, sources, and high-resolution THz spectrometers [13]. It is also important to devise THz clocks for astronomical

instruments, especially astronomical interferometers and next-generation space telescopes for probing unexplored areas of the universe, including our galaxy, in which more than 50% of the total luminosity is due to THz radiation [14,15]. Furthermore, the realization of the THz-frequency standard is necessary to understand star formation and decay processes, as well as the thermal fluctuations in the environment due to the immense release of greenhouse gases [14].

The proposition of implementing absolute-frequency standards in the THz domain was first introduced in 1972 by Strumia, who considered fine-structure transition lines of Mg and Ca metastable triplet states [16]. Yamamoto *et al.* first generated a tunable THz optical clock with a 100 GHz to 1 THz frequency range [17]. Champenois *et al.* first proposed the THz-frequency standard based on three-photon coherent population trapping in trapped-ion clouds [18]. Zhou *et al.* considered alkaline-earth atoms, including Sr, Ca, and Mg, to determine the magic wavelengths of THz clock transitions between their metastable triplet states [19]. Yu *et al.* evaluated ac Stark shifts and magic wavelengths of THz clock transitions in barium [20]. Wang *et al.* probed carbonyl sulfide (OCS) to realize two different molecular clocks based on the sub-THz-frequency standard [21]. The miniaturization of atomic clocks with high affordability to chip-scale THz OCS clocks was analyzed by Kim *et al.* [12], whereas Drake *et al.* considered silicon nitride to analyze the performance of THz-rate Kerr microresonator optical clocks [22]. Wang *et al.* proposed chip-scale molecular clocks based on a complementary-metal-oxide-semiconductor technique with selected OCS transitions [23]. A THz molecular clock using vibrational levels of Sr_2 was constructed by Leung *et al.* [24], who achieved systematic uncertainty at the level of 10^{-14} .

*Contact author: jbchen@pku.edu.cn†Contact author: bijaya@prl.res.in

minimal implementation of lasers in the scheme. To achieve the high stability and high accuracy in this proposed THz-clock scheme, using a feedback loop to control the energy difference between the $4D_{3/2}$ and $4D_{5/2}$ states is recommended. This feedback loop would adjust the static magnetic field applied to the ion trap to maintain a stable clock frequency over time [37]. All these characteristics of Nb^{4+} ensure that it is a viable candidate for a THz clock.

III. METHOD OF EVALUATION

Precise determination of systematic frequency shifts in a clock transition requires accurate computation of the wave functions of the involved states. Therefore, we implement relativistic-coupled-cluster (RCC) theory for accurate computation of these wave functions as well as the matrix elements of physical operators. Higher-order correlations due to various physical effects accounting for core-polarization and pair-correlation effects are also incorporated through the nonlinear terms of the RCC theory. Although the general formulation and potential applications of RCC theory can be found in many previous studies, including Refs. [38–42], we provide a brief outline of our employed RCC method below.

We begin with the Dirac-Coulomb Hamiltonian H_{DC} in our RCC method, which in atomic units is given by

$$H_{\text{DC}} = \sum_{i=1}^{N_e} [c\vec{\alpha}_D \cdot \vec{p}_i + (\beta - 1)c^2 + V_n(r_i)] + \sum_{i>j} \frac{1}{r_{ij}}, \quad (1)$$

where N_e is the number of electrons in the atom, c is the speed of light, $\vec{\alpha}_D$ and β are the 4×4 Dirac matrices, $V_n(r)$ is the nuclear potential, and r_{ij} is the interelectronic distance between electrons located at r_i and r_j . Corrections due to Breit and lower-order quantum electrodynamics (QED) are also included to improve accuracy in our calculations [43–46]. Note that contributions from the negative-energy states (NESs) are neglected here, which will not affect our results in the precision of interest.

In the RCC-theory ansatz, the wave function of a many-electron system can be expressed in terms of the mean-field (MF) wave function $|\Phi_0\rangle$ of an atomic state and cluster operator T as [47]

$$|\Psi_0\rangle = e^T |\Phi_0\rangle. \quad (2)$$

By solving the Dirac-Fock (DF) equation for the closed-shell configurations ($[4p^6]$), we get the MF wave function $|\Phi_0\rangle$, and then, we obtain the DF wave function $|\Phi_v\rangle$ of the state with configuration $[4p^6]v$ by adding a suitable valence orbital v . In terms of the creation operator for the valence electron a_v^\dagger , it is given as [48]

$$|\Phi_v\rangle = a_v^\dagger |\Phi_0\rangle. \quad (3)$$

The wave function of an atomic state with a closed-shell electronic configuration and a valence orbital can be expressed in terms of a RCC operator that accounts for the excitations of core electrons to virtual orbitals T and the operator S_v , which accounts for the excitation of the valence orbital to a virtual orbital as [41]

$$|\Psi_v\rangle = e^T \{1 + S_v\} |\Phi_v\rangle, \quad (4)$$

where T and S_v can account for the singly and doubly excited-state configurations in our RCC-theory (RCCSD method) ansatz as [41]

$$T = T_1 + T_2, \quad S_v = S_{1v} + S_{2v}. \quad (5)$$

Accounting for excitations from both the core and valence orbitals of DF wave functions of the Nb^{4+} ion, we define the T and S_v operators in terms of the second-quantization operators and their amplitudes ρ as [49]

$$\begin{aligned} T_1 &= \sum_{p,a} \rho_{pa} a_p^\dagger a_a, & T_2 &= \frac{1}{4} \sum_{pq,ab} \rho_{pqab} a_p^\dagger a_q^\dagger a_b a_a, \\ S_{1v} &= \sum_{m \neq a} \rho_p a_p^\dagger a_v, & S_{2v} &= \frac{1}{2} \sum_{pq,a} \rho_{pqva} a_p^\dagger a_q^\dagger a_a a_v, \end{aligned} \quad (6)$$

where the indices p and q range over a large number of virtual orbitals with energies up to 3500 a.u. and the indices a and b range over all possible occupied orbitals.

Finally, the matrix elements of a physical operator \hat{O} between states k and v with the corresponding wave functions $|\Psi_v\rangle$ and $|\Psi_k\rangle$ are evaluated as [42,49]

$$\begin{aligned} O_{vk} &= \frac{\langle \Psi_v | \hat{O} | \Psi_k \rangle}{\sqrt{\langle \Psi_v | \Psi_v \rangle \langle \Psi_k | \Psi_k \rangle}} \\ &= \frac{\langle \Phi_v | \{S_v^\dagger + 1\} \bar{\hat{O}} \{1 + S_k\} | \Phi_k \rangle}{\langle \Phi_v | \{S_v^\dagger + 1\} \bar{N} \{1 + S_k\} | \Phi_k \rangle}, \end{aligned} \quad (7)$$

where $\bar{\hat{O}} = e^{T^\dagger} \hat{O} e^T$ and $\bar{N} = e^{T^\dagger} e^T$, with $\bar{\hat{O}}$ and \bar{N} being nonterminating series. In Eq. (7), \hat{O} can be replaced by the $E1$, $M1$, and electric quadrupole ($E2$) operators, depending upon the matrix elements that need to be evaluated for the analysis.

In this work, we use Gaussian-type orbitals (GTOs) as the single-electron basis set in the calculations. The GTOs for the large (L) and small (S) components are given by [50–52]

$$\begin{aligned} g_{l,i}^L &= N^L r^{l+1} e^{-\eta_i r^2}, \\ g_{l,i}^S &= N^S \left[\frac{d}{dr} + \frac{\kappa}{r} \right] g_{l,i}^L. \end{aligned} \quad (8)$$

Here, $N^{L,S}$ represents the normalization constant for the L and S components, η_i is an arbitrary coefficient suitably chosen for accurate calculations of wave functions, l is the orbital quantum number, and κ is the relativistic quantum number. The exponents η_i are determined by the relation $\eta_i = \eta_0 \beta^{i-1}$. We use a large basis set of functions with 40, 39, 38, 37, 36, 35, and 34 GTOs for the s , p , d , f , g , h , and i orbitals, respectively. We list the η_0 and β parameters that are used in the present calculations for each symmetry in Table I.

IV. ESTIMATION OF ENERGIES

In order to find the accuracy of the wave functions from the RCCSD method used to determine various matrix elements, we present energies obtained with this method in Table II. Contributions from the Breit and QED corrections to the calculated energies are also shown explicitly. Table II shows that the Breit and QED contributions are within 0.01% of the

TABLE I. List of η_0 and β parameters used to define the GTOs for different symmetries to construct single-particle orbitals in the present calculations.

	s	p	d	f	g	h	i
η_0	0.0009	0.0008	0.001	0.004	0.005	0.005	0.005
β	2.15	2.15	2.15	2.25	2.35	2.35	2.35

total calculated values. The final calculated values are also compared with those tabulated in the NIST database [53]. We find about 0.5% variation between our calculated energies and NIST data.

V. DIPOLE POLARIZABILITIES

Interaction of an atomic or ionic system with external electromagnetic fields leads to electric and magnetic polarization of the system. This causes the shifts in energy levels of the considered atomic system, which can be estimated to second order by evaluating electric and magnetic dipole polarizabilities of the considered states. Thus, accurate determination of the $E1$ and $M1$ polarizabilities is essential in order to estimate

possible systematics in the clock states of the considered atomic system. It requires determination of the $E1$ and $M1$ matrix elements and energies. The required matrix elements are evaluated using the aforementioned RCC method, whereas excitation energies are taken from the NIST database [53] in this work. Further details of these calculations and the obtained results are discussed below.

A. Evaluation of $E1$ polarizabilities

The total $E1$ polarizability $\alpha_{F_n}^{E1}(\omega)$ of any hyperfine state $|F_n, M_F\rangle$ at any frequency ω for linearly polarized light for the off-resonant spectrum can be represented in terms of scalar and tensor components as [54–57]

$$\alpha_{F_n}^{E1}(\omega) = \alpha_{n0,F_n}^{E1}(\omega) + \frac{3M_F^2 - F_n(F_n + 1)}{F_n(2F_n - 1)} \alpha_{n2,F_n}^{E1}(\omega). \quad (9)$$

Further, the scalar $\alpha_{n0,F_n}^{E1}(\omega)$ and tensor $\alpha_{n2,F_n}^{E1}(\omega)$ components are given in terms of total angular momentum (J_n) dependent polarizabilities by

$$\alpha_{n0,F_n}^{E1}(\omega) = \alpha_{n0,J_n}^{E1}(\omega) \quad (10)$$

and

$$\alpha_{n2,F_n}^{E1}(\omega) = (-1)^{J_n+F_n+I} \begin{Bmatrix} F_n & J_n & I \\ J_n & F_n & 2 \end{Bmatrix} \alpha_{n2,J_n}^{E1}(\omega) \sqrt{\frac{F_n(2F_n - 1)(2F_n + 1)(2J_n + 3)(2J_n + 1)(J_n + 1)}{(2F_n + 3)(F_n + 1)(J_n)(2J_n - 1)}}. \quad (11)$$

Since calculating hyperfine-level wave functions is challenging, the F -dependent dynamic polarizability for linearly polarized light can be determined using Eq. (9) for the atomic $E1$ polarizabilities. In the above expressions, $\alpha_{n0,J_n}^{E1}(\omega)$ and $\alpha_{n2,J_n}^{E1}(\omega)$ can be determined using the relations

$$\alpha_{n0,J_n}^{E1}(\omega) = -\frac{1}{3(2J_n + 1)} \sum_{J_k} |\langle J_n || \mathbf{D} || J_k \rangle|^2 \times \left[\frac{1}{\delta E_{nk} + \omega} + \frac{1}{\delta E_{nk} - \omega} \right] \quad (12)$$

and

$$\alpha_{n2,J_n}^{E1}(\omega) = 2 \sqrt{\frac{5J_n(2J_n - 1)}{6(J_n + 1)(2J_n + 3)(2J_n + 1)}} \times \sum_{J_k} (-1)^{J_k+J_n+1} \begin{Bmatrix} J_n & 2 & J_n \\ 1 & J_k & 1 \end{Bmatrix} \times |\langle J_n || \mathbf{D} || J_k \rangle|^2 \left[\frac{1}{\delta E_{nk} + \omega} + \frac{1}{\delta E_{nk} - \omega} \right]. \quad (13)$$

Here, $|\langle J_n || \mathbf{D} || J_k \rangle|$ are the reduced electric dipole matrix elements (reduced using the Wigner–Eckart theorem), with \mathbf{D} being the electric dipole ($E1$) operator, J_k being the angular momentum of the intermediate state k , and $\delta E_{nk} = E_n - E_k$, where E_i^0 corresponds to the unperturbed energies of the states for $i = n, k$. The terms in curly bracket in Eqs. (11) and (13) refer to 6- j symbols. The static values of the $E1$ polarizabilities can be deduced by substituting $\omega = 0$ in the above expressions.

The above expressions for the $E1$ polarizabilities can be used to estimate contributions from the low-lying intermediate states whose matrix elements can explicitly be determined. To account for contributions from the core and continuum orbitals, we divide them into core (α^c), core-valence (α^{vc}), and valence (α^{val}) correlations, as discussed in Ref. [58]. Contributions from the virtual intermediate states correspond to α^{val} , which are further divided into “main” and “tail” contributions from the low-lying virtual states and high-lying virtual states, respectively. Contributions from the core orbitals without and with valence orbital interactions are given by α^c and α^{vc} , respectively. Thus, we can write

$$\alpha^{RCC} = \alpha^c + \alpha^{vc} + \alpha^{val}, \quad (14)$$

where $\alpha^{val} = \alpha_{Main}^{val} + \alpha_{Tail}^{val}$.

To verify the roles of the Breit and QED interactions in the determination of the $E1$ polarizabilities, we present the final value of α^{E1} as

$$\alpha^{E1} = \alpha^{RCC+Breit+QED}. \quad (15)$$

As mentioned above, energies are taken from the NIST data in the evaluation of the main contributions. NES contributions to the length-gauge expression for the $E1$ matrix elements are negligible [59,60]; thus, contributions from the NESs to the final α^{E1} values are expected to be small.

The results for J -dependent static $E1$ polarizabilities ($\omega = 0$) of the $4D_{3/2}$ and $4D_{5/2}$ states from the off-resonant lasing spectra are listed in Table III. From these results, it can be observed that the $4D_{3/2}-5P_{1/2,3/2}$ and $4D_{3/2}-4F_{5/2}$

TABLE II. Estimated energies (in cm^{-1}) of various states of the Nb^{4+} ion and their comparison with available NIST values. The percent deviation $\delta(\%)$ is also provided. Values in square brackets depict the order of 10.

Source	$4D_{3/2}$	$4D_{5/2}$	$4F_{5/2}$	$4F_{7/2}$	$5S_{1/2}$	$5P_{1/2}$	$5P_{3/2}$	$6S_{1/2}$	$6P_{1/2}$	$6P_{3/2}$
RCC	407 832.95	405 874.28	191 705.65	191 631.10	332 251.04	278 918.66	275 246.78	179 435.61	157 407.86	155 865.40
+Breit	37.10	118.95	53.42	58.32	-67.19	-112.15	-56.71	-27.85	-47.92	-24.78
+QED	36.25	32.79	5.13	4.89	-84.64	6.35	3.23	-32.26	2.46	1.19
Total	407 906.30	406 026.02	191 764.20	191 694.31	332 099.21	278 812.90	275 193.30	179 375.5	157 362.40	155 841.81
NIST	407 897.00	406 029.60	192 637.90	192 499.50	331 967.40	278 701.80	275 097.00	179 400.70	157 390.50	155 873.70
$\delta(\%)$	2.28[-3]	8.86[-4]	4.54[-1]	4.18[-1]	3.97[-2]	3.99[-2]	3.50[-2]	1.40[-2]	1.79[-2]	2.05[-2]

transitions contribute dominantly to the static $E1$ polarizabilities of the $4D_{3/2}$ state, whereas the $4D_{5/2}-5P_{3/2}$ and $4D_{5/2}-4F_{5/2,7/2}$ transitions contribute majorly to the static $E1$ polarizability of the $4D_{5/2}$ state. As shown in Eq. (10), the scalar components of the $E1$ polarizability for both the atomic and hyperfine levels are equal; thus, it can safely be deduced that the static scalar $E1$ polarizabilities α_{n0,F_n}^{E1} for the $4D_{3/2}[[3, \pm 2]]$ and $4D_{5/2}[[3, \pm 2]]$ hyperfine levels are 3.1429 and 3.1506 a.u., respectively. In order to validate the accuracy of our results, we compare our results with the static dipole polarizability values estimated using the RCC method without Breit and QED corrections as well as the third-order relativistic many-body perturbation theory (RMBPT3)

method incorporating major physical correlations specifically through the random-phase approximation, Brückner orbitals, structural radiations, and the normalization of wave functions. The comparison of the results shows underlying uncertainties $\delta_1(\%)$ and $\delta_2(\%)$ less than 0.5% and 10% with respect to the RCC and RMBPT3 methods, respectively. The high uncertainty in comparison with the RMBPT3 method is expected due to the fact that this method incorporates only major physical correlations up to third order. In addition, when we include the near-resonant lasing spectra, it is observed that the linewidths of the contributing states to the $E1$ polarizabilities are negligibly small (of the order of 10^{-6} or less).

 TABLE III. Contributions from different dominant far-off resonant transitions to the static dipole polarizabilities (in a.u.) of the $4D_{3/2}$ and $4D_{5/2}$ states of the Nb^{4+} ion. Percent deviations $\delta_1(\%)$ and $\delta_2(\%)$ represent the deviation in the RCC+Breit+QED results with the RCC and RMBPT3 results, respectively. Here, values under d denote the $E1$ matrix elements. $\alpha_{w0}(0)$ and $\alpha_{w2}(0)$ correspond to the scalar and tensor components, respectively, of the $E1$ polarizability for the $4D_{3/2}$ state, while $\alpha_{v0}(0)$ and $\alpha_{v2}(0)$ denote the same for the $4D_{5/2}$ state.

$4D_{3/2}$				$4D_{5/2}$			
Transition	d	$\alpha_{w0}(0)$	$\alpha_{w2}(0)$	Transition	d	$\alpha_{v0}(0)$	$\alpha_{v2}(0)$
$4D_{3/2}-5P_{1/2}$	1.179	0.3936	-0.3936	$4D_{5/2}-5P_{3/2}$	1.569	0.4585	-0.4585
$4D_{3/2}-6P_{1/2}$	0.227	0.0075	-0.0075	$4D_{5/2}-6P_{3/2}$	0.319	0.0099	-0.0099
$4D_{3/2}-7P_{1/2}$	0.096	0.0011	-0.0011	$4D_{5/2}-7P_{3/2}$	0.158	0.0020	-0.0020
$4D_{3/2}-8P_{1/2}$	0.065	0.0005	-0.0005	$4D_{5/2}-8P_{3/2}$	0.095	0.0007	-0.0007
$4D_{3/2}-9P_{1/2}$	0.034	0.0001	-0.0001	$4D_{5/2}-9P_{3/2}$	0.063	0.0003	0.0003
$4D_{3/2}-10P_{1/2}$	0.028	0.0001	-0.0001	$4D_{5/2}-10P_{3/2}$	0.045	0.0001	0.0001
$4D_{3/2}-5P_{3/2}$	0.515	0.0730	0.0584	$4D_{5/2}-4F_{5/2}$	0.480	0.0263	0.0301
$4D_{3/2}-6P_{3/2}$	0.106	0.0016	0.0013	$4D_{5/2}-5F_{5/2}$	0.064	0.0004	0.0005
$4D_{3/2}-7P_{3/2}$	0.053	0.0003	0.0002	$4D_{5/2}-6F_{5/2}$	0.043	0.0001	0.0001
$4D_{3/2}-8P_{3/2}$	0.032	0.0001	0.0001	$4D_{5/2}-4F_{7/2}$	2.158	0.5318	-0.1899
$4D_{3/2}-9P_{3/2}$	0.021	0.0	0.0	$4D_{5/2}-5F_{7/2}$	0.303	0.0081	-0.0029
$4D_{3/2}-10P_{3/2}$	0.015	0.0	0.0	$4D_{5/2}-6F_{7/2}$	0.167	0.0021	-0.0008
$4D_{3/2}-4F_{5/2}$	1.770	0.5324	-0.1065				
$4D_{3/2}-5F_{5/2}$	0.237	0.0074	-0.0015				
$4D_{3/2}-6F_{5/2}$	0.157	0.0028	-0.0006				
$4D_{3/2}-7F_{5/2}$	0.311	0.0105	-0.0021				
$4D_{3/2}-8F_{5/2}$	0.265	0.0073	-0.0015				
$\alpha_{\text{Main}}^{\text{val}}$		1.0383	-0.4551	$\alpha_{\text{Main}}^{\text{val}}$		1.0403	-0.6336
$\alpha_{\text{Tail}}^{\text{val}}$		0.0393	-0.0110	$\alpha_{\text{Tail}}^{\text{val}}$		0.0603	-0.0216
α^{vc}		-0.2148	0.1450	α^{vc}		-0.2297	0.2297
α^{c}		2.2780		α^{c}		2.2780	
RCC		3.1408	-0.3211	RCC		3.1489	-0.4255
RCC+Breit+QED (α^{E1})		3.1429	-0.3201	RCC+Breit+QED (α^{E1})		3.1506	-0.4251
RMBPT3		3.3540	-0.3406	RMBPT3		3.3766	-0.4105
$\delta_1(\%)$		0.07	0.31	$\delta_2(\%)$		0.05	0.09
$\delta_2(\%)$		6.79	6.40	$\delta_1(\%)$		7.17	3.43

B. Evaluation of $M1$ Polarizabilities

The interaction of magnetic dipoles μ_m within an ionic system with an external magnetic field \mathcal{B} leads to the magnetic polarization of the system. These magnetic interactions can be addressed quantum mechanically, using the $M1$ operator $\hat{O}^{M1} = (\mathbf{L} + 2\mathbf{S})\mu_B$ for Russell-Saunders coupling, with μ_B being the Bohr magneton and \mathbf{L} and \mathbf{S} being the orbital and spin angular momentum operators, respectively. Quantitatively, the phenomenon of magnetic polarization can be described through the physical quantity α_{n,F_n}^{M1} , generally known as magnetic dipole polarizability, which, for any hyperfine state n , can be expressed as [61]

$$\alpha_{n,F_n}^{M1} = -\frac{2}{3(2F_n + 1)} \sum_k \frac{|\langle F_n || \hat{O}^{M1} || F_k \rangle|^2}{E_{F_n} - E_{F_k}}, \quad (16)$$

where \hat{O}^{M1} is the $M1$ operator and F_k represents the intermediate hyperfine states to which all the allowed transitions from F_n are possible. In Eq. (16), energies of the hyperfine levels can be estimated by [62]

$$E_{F_n} = \frac{A_{\text{hf}}}{2} K_n + B_{\text{hf}} \left[\frac{\frac{3}{4} K_n (K_n + 1) - I(I + 1) J_n (J_n + 1)}{2I(2I - 1) J_n (2J_n - 1)} \right], \quad (17)$$

where $K_n = F_n(F_n + 1) - J_n(J_n + 1) - I(I + 1)$ and A_{hf} and B_{hf} are the $M1$ and $E2$ hyperfine interaction constants for the considered states, respectively, which are given by [62]

$$A_{\text{hf}} = \mu_N g_I \frac{\langle J_n || \hat{O}_{\text{hf}}^{(1)} || J_n \rangle}{\sqrt{J_n(J_n + 1)(2J_n + 1)}} \quad (18)$$

and

$$B_{\text{hf}} = 2Q \left[\frac{2J_n(2J_n - 1)}{(2J_n + 1)(2J_n + 2)(2J_n + 3)} \right]^{\frac{1}{2}} \langle J_n || \hat{O}_{\text{hf}}^{(2)} || J_n \rangle, \quad (19)$$

where μ_N is the nuclear Bohr magneton; $g_I = \frac{\mu_I}{I}$, with nuclear $M1$ moment μ_I and nuclear spin I ; and Q is the nuclear $E2$ moment. In Eqs. (18) and (19), $\hat{O}_{\text{hf}}^{(1)}$ and $\hat{O}_{\text{hf}}^{(2)}$ depict hyperfine operators given in the form [63]

$$\hat{O}_{\text{hf}}^{(1)} = \sum_j -ie \sqrt{\frac{8\pi}{3}} \frac{1}{r_j^2} \alpha_j Y_{1q}^{(0)}(r_j) \quad (20)$$

and

$$\hat{O}_{\text{hf}}^{(2)} = \sum_j -ie \frac{1}{r_j^3} C_q^{(2)}(r_j), \quad (21)$$

where q represents the order of spherical harmonics and functions Y and C are the tensor operators, with respective orders given in parentheses in the superscripts. Further, the reduced F -dependent $M1$ matrix elements (reduced using the Wigner-Eckart theorem) in Eq. (16) can easily be determined by using J -dependent $M1$ matrix elements as [48,64]

$$\begin{aligned} \langle F_n || \hat{O}^{M1} || F_k \rangle &= \sqrt{(2F_n + 1)(2F_k + 1)} \\ &\times \begin{Bmatrix} J_n & I & F_n \\ F_k & 1 & J_n \end{Bmatrix} \langle J_n || \hat{O}^{M1} || J_k \rangle. \end{aligned} \quad (22)$$

Contributions from the Breit and QED effects to the calculated $M1$ matrix elements are found to be extremely small. The uncertainties of the $M1$ polarizabilities mostly rely on the estimated energy differences which are determined from the calculated hyperfine structure constants using the RCCSD method. These uncertainties will dominate over the contributions from the NESs. Again, it has been shown that contributions from NESs to the evaluation of the $M1$ matrix elements drastically decrease with increasing atomic number [60,65]. Therefore, NES contributions to the evaluation of $M1$ polarizabilities can be safely neglected here.

On the basis of the selection rules of the $M1$ transition, it is found that the $4D_{3/2}|F=3\rangle \rightarrow 4D_{3/2}|F=4\rangle$ transition is the primary contributor to the $M1$ polarizability of the $4D_{3/2}|F=3\rangle$ state, with an estimated value of $2.6836 \times 10^{-23} \text{ J T}^{-2}$. Similarly, for the $4D_{5/2}|F=3\rangle$ state, the $4D_{5/2}|F=3\rangle \rightarrow 4D_{5/2}|F=2,4\rangle$ transitions contribute to its $M1$ polarizability, yielding a value of $9.0125 \times 10^{-23} \text{ J T}^{-2}$. Eventually, the validation of our results is based on the comparison of our results to the α^{M1} values obtained using the RCC and RMBPT3 methods, resulting in corresponding percent deviations of 1.86% and 4.55% and 3.65% and 4.59% for the $4D_{3/2}$ and $4D_{5/2}$ states, respectively.

VI. ESTIMATION OF MAJOR SYSTEMATIC SHIFTS TO CLOCK STATES

We now estimate and discuss major systematics that contribute mostly to the uncertainty of the clock-frequency measurement. We use the calculated quantities discussed in the previous section to estimate the BBR, Zeeman, electric quadrupole, and Doppler shifts. All these estimations are summarized in Table IV and are discussed below.

A. BBR shifts

The impact of the temperature T of the environment on the clock-frequency measurement is prevalent and leads to thermal fluctuations of the electromagnetic field. These thermal fluctuations are further experienced by an atomic system, resulting in the interaction of the system with both electric- and magnetic-field components of blackbody radiation, thus inducing the shifts in the energy states, generally known as BBR Stark (BBRS) and BBR Zeeman (BBRZ) shifts, respectively. They are one of the major irreducible contributions to the uncertainty of any atomic clock [66,67].

Considering a system at room temperature $T = 300 \text{ K}$, the BBRS shift of an energy level can be expressed in terms of the differential static scalar polarizability $\Delta\alpha_0^{E1} = \alpha_{v0,F_v}^{E1} - \alpha_{w0,F_w}^{E1}$ of the considered clock transition as [68]

$$\Delta v_{\text{BBR}}^{E1} = -\frac{1}{2h} (831.9 \text{ V/m})^2 \Delta\alpha_0^{E1}, \quad (23)$$

where the $E1$ polarizability α_{n0,F_n}^{E1} in atomic units can be converted into SI units using $\alpha/h [\text{Hz(V/m)}^{-2}] = 2.48832 \times 10^{-8} \alpha \text{ (a.u.)}$.

Similarly, the BBRZ shift due to the differential $M1$ polarizability $\Delta\alpha^{M1}$ of the clock transition is given by [69]

$$\Delta v_{\text{BBR}}^{M1} = -\frac{1}{2h} (2.77 \times 10^{-6} \text{ T})^2 \Delta\alpha^{M1} \quad (24)$$

TABLE IV. Estimated systematic shifts in the $4D_{3/2}|3, \pm 2\rangle - 4D_{5/2}|3, \pm 2\rangle$ THz clock transition of the Nb^{4+} ion.

Source	$\Delta\nu$ (Hz)	$\frac{\Delta\nu}{\nu_0}$
Electric quadrupole	0	0
BBR Zeeman ($T = 300$ K)	-0.3664	-6.5402×10^{-15}
BBR Stark ($T = 300$ K)	-6.6299×10^{-5}	-1.1834×10^{-18}
Quadratic Zeeman ($B = 10^{-8}$ T)	-5.1197×10^{-6}	-9.1387×10^{-20}
Second-order Doppler (Thermal)	-2.5081×10^{-14}	-4.4769×10^{-28}

at 300 K. Here, $\Delta\alpha^{M1} = \alpha_{v,F_v}^{M1} - \alpha_{w,F_w}^{M1}$ (in units of μ_B) can be converted to SI units using the relation $1\mu_B = 9.274 \times 10^{-24} \text{ J T}^{-1}$.

From Table III, it can be seen that the scalar static $E1$ polarizabilities α_{n0,F_n}^{E1} for the $4D_{3/2}|3, \pm 2\rangle$ and $4D_{5/2}|3, \pm 2\rangle$ hyperfine levels are about 3.1429 and 3.1506 a.u., respectively. Thus, the differential static $E1$ polarizability is estimated to be 7.7000×10^{-3} a.u., resulting in BBRS and fractional BBRS shifts of -6.6299×10^{-5} Hz and -1.1834×10^{-18} , respectively, with uncertainties of 5.19% and 5.20% with respect to BBRS and fractional BBRS shifts evaluated using only the RCC method. However, for the BBRZ shift, the evaluated $M1$ polarizabilities for the $4D_{3/2}|F = 3\rangle$ and $4D_{5/2}|F = 3\rangle$ hyperfine levels are found to be 2.6836×10^{-23} and $9.0125 \times 10^{-23} \text{ J T}^{-2}$, respectively, with corresponding uncertainties of 1.86% and 4.55% with respect to the $M1$ polarizability values evaluated using only the RCC approach. This corresponds to a BBRZ shift $\Delta\nu_{\text{BBR}}^{M1}$ of -0.3664 Hz with an uncertainty of -0.0029 Hz, whereas the fractional BBRZ shift is found to be -6.5402×10^{-15} , resulting in an estimated uncertainty of -5.1765×10^{-17} with respect to the RCC results.

B. Zeeman shifts

The interaction of the $M1$ moment μ_B of an ion with an external magnetic beam of intensity \mathcal{B} causes significant shifts in the hyperfine energy levels as well as transition frequencies of the system, usually known as Zeeman shifts [70]. The linear Zeeman shifts can be avoided if the average is taken over the transition frequencies with positive and negative M_F states, as described in Refs. [71,72]. Although the first-order Zeeman shifts are avoidable, the quadratic Zeeman shifts can contribute significantly to the frequency uncertainty budget, and hence, they must be estimated. The quadratic Zeeman shift to the clock transition can be expressed in terms of differential $M1$ polarizability $\Delta\alpha^{M1}$ as [73]

$$\Delta\nu^{(Z2)} = -\frac{1}{2h}\Delta\alpha^{M1}\mathcal{B}^2, \quad (25)$$

with $\Delta\alpha^{M1} = \alpha_{v,F_v}^{M1} - \alpha_{w,F_w}^{M1}$. Substituting the $M1$ polarizability values of 2.6336×10^{-23} and $9.4223 \times 10^{-23} \text{ J T}^{-2}$, corresponding to the $4D_{3/2}|F = 3\rangle$ and $4D_{5/2}|F = 3\rangle$ hyperfine levels, leads to a quadratic Zeeman shift $\Delta\nu^{(Z2)}$ and fractional Zeeman shift of the clock transition of -5.1197×10^{-6} Hz and -9.1387×10^{-20} , respectively.

C. Electric quadrupole shifts

The interaction of quadrupole moments of the clock levels with the residual electric-field gradient at the trap center can

be described using the Hamiltonian H_Q [74], given by

$$H_Q = \nabla\mathbf{E}^{(2)} \cdot \mathbf{\Theta}^{(2)}, \quad (26)$$

where $\nabla\mathbf{E}^{(2)}$ is the tensor describing the gradient of external electric field and $\mathbf{\Theta}^{(2)}$ is the electric quadrupole operator for the considered ion. This interaction further leads to a shift in the energies of the clock levels, which can be estimated using [75]

$$\Delta E \simeq -\frac{1}{2}\Delta\langle Q_0 \rangle \frac{\partial \mathcal{E}_z}{\partial z}. \quad (27)$$

In Eq. (27), $\langle Q_0 \rangle \equiv \langle \gamma JIFM | \mathbf{\Theta}^{(2)} | \gamma JIFM \rangle$, with γ including all other quantum numbers. The expectation value $\langle Q_0 \rangle$ of any state n can be evaluated using [74]

$$\begin{aligned} \langle \gamma JIFM | Q_0 | \gamma JIFM \rangle &= (-1)^{J+J_n+F_n} [3M_F^2 - F_n(F_n + 1)] \\ &\times \sqrt{\frac{2F_n + 1}{(2F_n + 3)(F_n + 1)(2F_n - 1)}} \\ &\times \begin{Bmatrix} J_n & J_n & 2 \\ F_n & F_n & I \end{Bmatrix} \times \langle \gamma J | \mathbf{\Theta}^{(2)} | \gamma J \rangle, \end{aligned} \quad (28)$$

with $\langle \gamma J | \mathbf{\Theta}^{(2)} | \gamma J \rangle$ being the reduced matrix element of the quadrupole operator. From Eq. (28), it can easily be deduced that minimization of the electric quadrupole shift can be observed if $3M_F^2 - F_n(F_n + 1) = 0$, implying $3M_F^2 = F_n(F_n + 1)$. Since Nb^{4+} has nuclear spin, $I = \frac{9}{2}$; thus, the total angular momentum F acquires values of 3–6 and 2–7 for the $4D_{3/2}$ and $4D_{5/2}$ states, respectively. Therefore, the electric quadrupole shifts for both of these clock levels can be nullified when $|F, M_F\rangle$ are chosen to be $|3, \pm 2\rangle$. That is the reason why we selected the $|3, \pm 2\rangle$ hyperfine levels in the scheme shown in Fig. 1 for the clock-frequency measurement.

D. Doppler shift

Doppler shifts occur due to the distribution of velocity among the considered atomic systems in the experiment when an atomic-clock system is operated on a particular temperature [76]. The cold, but moving, ions in this case can interact with the field inside the microwave cavity with a spatial phase variation, thereby shifting the energy levels involved in the clock transition [77]. The accuracy of the atomic clock is limited by these Doppler shifts; hence, it is necessary to minimize both the first- and second-order Doppler shifts for high-precision clock-frequency measurement. The first-order Doppler shift can be eliminated by using two probe beams in opposite directions during the detection [78]; however, the second-order Doppler shift due to secular motion is quite

considerable and can be as large as 1 part in 10^8 [77]. This second-order Doppler shift can be expressed in terms of the mass m of the considered ion and speed of light c in vacuum as [79]

$$\Delta\nu_{D2} = -\left(\frac{3\hbar\Gamma}{4mc^2}\right)v_0. \quad (29)$$

Considering the current advanced experimental techniques, we recommend using cooling lasers under optimized working conditions to cool the ion trap to a temperature closer to the Doppler-cooling limit T_D . Acquiring temperature near T_D , the second-order Doppler shift due to the secular motion of the ion can further be minimized [80]. This Doppler-cooling limit depends on the natural linewidth of the atomic transition Γ^{-1} and is determined using the formula [81]

$$T_D = \frac{\hbar\Gamma}{2K_B}. \quad (30)$$

Here, Γ is the rate of spontaneous emission of the excited state and is given by $\Gamma = \frac{1}{\tau_v}$, where v corresponds to the excited state. Substituting the value of the Doppler-cooling limit from Eq. (30) in Eq. (29), we get

$$\Delta\nu_{D2} = -\left(\frac{3K_B T_D}{2mc^2}\right)v_0. \quad (31)$$

For Nb^{4+} , the lifetime of the excited state, i.e., $\tau_{4D_{5/2}} = 12.65$ s, results in a Doppler-cooling limit of 0.302 pK. Consequently, if we substitute the value of T_D in Eq. (31), the second-order Doppler shift and fractional frequency shift are found to be -2.5081×10^{-14} Hz and -4.4769×10^{-28} , respectively.

It is obvious from the above results that the BBRZ shift contributes at the 10^{-15} level, while other systematic effects can contribute below 10^{-17} . The uncertainty due to the BBRZ shift can be reduced further by performing the experiment at lower temperatures or measuring the $M1$ polarizability more precisely. Nonetheless, the large value of the BBRZ shift can be useful. Since it is highly sensitive to magnetic-field

fluctuations, the Nb^{4+} ion clock can be utilized for quantum thermometry.

VII. CONCLUSION

This work demonstrated that the $4D_{3/2}|F=3, M_F=\pm 2\rangle \rightarrow 4D_{5/2}, |F=3, M_F=\pm 2\rangle$ transition in the $^{93}\text{Nb}^{4+}$ ion can work as a prospective terahertz atomic clock. In view of this, we explicitly discussed our clock proposal and evaluated major systematics in this transition, including BBR, electric quadrupole, second-order Doppler, and second-order Zeeman shifts. The maximum contribution to the systematics of this transition was observed to be contributed by external magnetic effects leading to considerable BBR Zeeman and quadratic Zeeman shifts. The minimization of other systematic shifts can be carried out by optimizing the parameters as suggested in the study. We also conclude that the Nb^{4+} THz clock is more sensitive to external magnetic fields in comparison to our previously proposed Zr^{3+} THz clock. Moreover, this clock scheme is independent of the ac Stark shift and electric quadrupole shift, which makes its implementation more favorable for experimentalists. Therefore, we expect it to be more useful for evolving quantum thermometry techniques as well as for evolving terahertz devices, including sources, detectors, and THz spectrometers, upon the successful implementation and development in an optimized environment.

ACKNOWLEDGMENTS

This research was funded by the Innovation Program for Quantum Science and Technology (Grant No. 2021ZD0303200) and the National Natural Science Foundation of China (Grant No. 624B2010). Research at Perimeter Institute is supported in part by the Government of Canada through the Department of Innovation, Science and Economic Development and by the province of Ontario through the Ministry of Colleges and Universities. We acknowledge the ParamVikram 1000 HPC facility at the Physical Research Laboratory, Ahmedabad, India, for carrying out relativistic coupled-cluster calculations. A.C. and B.K.S. were supported by the Department of Space, Government of India, to carry out this work. B.K.S. acknowledges ANRF for Grant No. CRG/2023/002558.

-
- [1] A. Derevianko and M. Pospelov, *Nat. Phys.* **10**, 933 (2014).
 - [2] T. Rosenband, D. Hume, P. Schmidt, C.-W. Chou, A. Brusch, L. Lorini, W. Oskay, R. E. Drullinger, T. M. Fortier, J. E. Stalnaker *et al.*, *Science* **319**, 1808 (2008).
 - [3] T. E. Mehlstäubler, G. Grosche, C. Lisdar, P. O. Schmidt, and H. Denker, *Rep. Prog. Phys.* **81**, 064401 (2018).
 - [4] W. McGrew, X. Zhang, R. Fasano, S. Schäffer, K. Beloy, D. Nicolodi, R. Brown, N. Hinkley, G. Milani, M. Schioppo *et al.*, *Nature (London)* **564**, 87 (2018).
 - [5] S. Kolkowitz, I. Pikovski, N. Langellier, M. D. Lukin, R. L. Walsworth, and J. Ye, *Phys. Rev. D* **94**, 124043 (2016).
 - [6] A. Loeb and D. Maoz, *arXiv:1501.00996*.
 - [7] P. W. Graham, J. M. Hogan, M. A. Kasevich, and S. Rajendran, *Phys. Rev. Lett.* **110**, 171102 (2013).
 - [8] V. A. Dzuba, V. V. Flambaum, and S. Schiller, *Phys. Rev. A* **98**, 022501 (2018).
 - [9] M. Tonouchi, *Nat. Photonics* **1**, 97 (2007).
 - [10] C. Kulesa, *IEEE Trans. Terahertz Sci. Technol.* **1**, 232 (2011).
 - [11] E. B. Norrgard, S. P. Eckel, C. L. Holloway, and E. L. Shirley, *New J. Phys.* **23**, 033037 (2021).
 - [12] M. Kim, C. Wang, Z. Hu, and R. Han, *IEEE Trans. Terahertz Sci. Technol.* **9**, 349 (2019).
 - [13] T. Yasui, S. Yokoyama, H. Inaba, K. Minoshima, T. Nagatsuma, and T. Araki, *IEEE J. Sel. Top. Quantum Electron.* **17**, 191 (2010).

- [14] L. Consolino, S. Bartalini, and P. De Natale, *J. Infrared Milli. Terahz. Waves* **38**, 1289 (2017).
- [15] M. Bellini, P. De Natale, G. Di Lonardo, L. Fusina, M. Inguscio, and M. Prevedelli, *J. Mol. Spectrosc.* **152**, 256 (1992).
- [16] F. Strumia, *Metrologia* **8**, 85 (1972).
- [17] T. Yamamoto, H. Takara, and S. Kawanishi, *2002 International Topical Meeting on Microwave Photonic, Awaji, Japan* (IEEE, Piscataway, NJ, 2002), pp. 97–100.
- [18] C. Champenois, G. Hagel, M. Houssin, M. Knoop, C. Zumsteg, and F. Vedel, *Phys. Rev. Lett.* **99**, 013001 (2007).
- [19] X. Zhou, X. Xu, X. Chen, and J. Chen, *Phys. Rev. A* **81**, 012115 (2010).
- [20] G.-H. Yu, Y.-G. Geng, L. Li, C. Zhou, C.-B. Duan, R.-P. Chai, and Y.-M. Yang, *Chin. Phys. B* **24**, 103201 (2015).
- [21] C. Wang, X. Yi, J. Mawdsley, M. Kim, Z. Wang, and R. Han, *Nat. Electron.* **1**, 421 (2018).
- [22] T. E. Drake, T. C. Briles, J. R. Stone, D. T. Spencer, D. R. Carlson, D. D. Hickstein, Q. Li, D. Westly, K. Srinivasan, S. A. Diddams *et al.*, *Phys. Rev. X* **9**, 031023 (2019).
- [23] C. Wang, X. Yi, M. Kim, Q. B. Yang, and R. Han, *IEEE J. Solid-State Circuits* **56**, 566 (2020).
- [24] K. H. Leung, B. Iritani, E. Tiberi, I. Majewska, M. Borkowski, R. Moszynski, and T. Zelevinsky, *Phys. Rev. X* **13**, 011047 (2023).
- [25] Jyoti, A. Chakraborty, Y. M. Yu, J. Chen, B. Arora, and B. K. Sahoo, *Phys. Rev. A* **108**, 023115 (2023).
- [26] Jyoti, M. Kaur, B. Arora, and B. K. Sahoo, *Mon. Not. R. Astron. Soc.* **507**, 4030 (2021).
- [27] A. Das, A. Bhowmik, N. N. Dutta, and S. Majumder, *J. Phys. B* **51**, 025001 (2018).
- [28] J. R. de Laeter, J. K. Böhlke, P. D. Bièvre, H. Hidaka, H. S. Peiser, K. J. R. Rosman, and P. D. P. Taylor, *Pure Appl. Chem.* **75**, 683 (2003).
- [29] J. Silver, A. Varney, H. Margolis, P. Baird, I. Grant, P. Groves, W. Hallett, A. Handford, P. Hirst, A. Holmes *et al.*, *Rev. Sci. Instrum.* **65**, 1072 (1994).
- [30] N. Nakamura, H. Kikuchi, H. A. Sakaue, and T. Watanabe, *Rev. Sci. Instrum.* **79**, 063104 (2008).
- [31] A. Agnihotri, A. Kelkar, S. Kasthurirangan, K. Thulasiram, C. Desai, W. Fernandez, and L. Tribedi, *Phys. Scr.* **2011**, 014038 (2011).
- [32] C. W. Chou, D. B. Hume, J. C. J. Koelemeij, D. J. Wineland, and T. Rosenband, *Phys. Rev. Lett.* **104**, 070802 (2010).
- [33] S. Hannig, L. Pelzer, N. Scharnhorst, J. Kramer, M. Stepanova, Z. T. Xu, N. Spethmann, I. D. Leroux, T. E. Mehlstäubler, and P. O. Schmidt, *Rev. Sci. Instrum.* **90**, 053204 (2019).
- [34] S. Micalizio, F. Levi, C. Calosso, M. Gozzelino, and A. Godone, *GPS Solutions* **25**, 94 (2021).
- [35] N. Wen, N. Zong, F.-F. Zhang, F. Yang, Z.-M. Wang, S.-J. Zhang, Y. Bo, Q.-J. Peng, D.-F. Cui, Z.-Y. Xu *et al.*, *Laser Phys. Lett.* **17**, 105001 (2020).
- [36] M. Singh, M. A. Fareed, R. G. Shirinabadi, R. Marcelino, F. Zhu, F. Légaré, and T. Ozaki, *Fundam. Plasma Phys.* **10**, 100043 (2024).
- [37] B. Merkel, K. Thirumalai, J. Tarlton, V. Schäfer, C. Ballance, T. Harty, and D. Lucas, *Rev. Sci. Instrum.* **90**, 044702 (2019).
- [38] S. A. Blundell, W. R. Johnson, and J. Sapirstein, *Phys. Rev. A* **43**, 3407 (1991).
- [39] E. E. (Ilyabaev), U. Kaldor, and Y. Ishikawa, *Chem. Phys. Lett.* **222**, 82 (1994).
- [40] E. Lindroth and A. Ynnerman, *Phys. Rev. A* **47**, 961 (1993).
- [41] B. K. Sahoo, S. Majumder, R. K. Chaudhuri, B. Das, and D. Mukherjee, *J. Phys. B* **37**, 3409 (2004).
- [42] D. K. Nandy and B. K. Sahoo, *Phys. Rev. A* **90**, 050503(R) (2014).
- [43] J. S. M. Ginges and J. C. Berengut, *Phys. Rev. A* **93**, 052509 (2016).
- [44] B. K. Sahoo, *Phys. Rev. A* **93**, 022503 (2016).
- [45] V. V. Flambaum and J. S. M. Ginges, *Phys. Rev. A* **72**, 052115 (2005).
- [46] C.-B. Li, Y. M. Yu, and B. K. Sahoo, *Phys. Rev. A* **97**, 022512 (2018).
- [47] J. Čížek, *Adv. Chem. Phys.* **14**, 35 (1969).
- [48] I. Lindgren and J. Morrison, *Atomic Many-Body Theory* (Springer, 2012), Vol. 3.
- [49] B. K. Sahoo, Ph.D. thesis, Mangalore University, Karnataka, India, 2005.
- [50] S. F. Boys, *Proc. R. Soc. London, Ser. A* **200**, 542 (1950).
- [51] S. Wilson, *Problem Solving in Computational Molecular Science: Molecules in Different Environments* (Springer, Netherlands, 1997), pp. 109–158.
- [52] A. K. Mohanty and E. Clementi, *Chem. Phys. Lett.* **157**, 348 (1989).
- [53] A. Kramida, Yu. Ralchenko, J. Reader, and NIST ASD Team, NIST Atomic Spectra Database, version 5.8, 2021, <https://physics.nist.gov/asd>.
- [54] N. L. Manakov, V. D. Ovsiannikov, and L. P. Rapoport, *Phys. Rep.* **141**, 320 (1986).
- [55] S. Singh, K. Kaur, B. Sahoo, and B. Arora, *J. Phys. B* **49**, 145005 (2016).
- [56] S. A. Schäffer, B. T. R. Christensen, S. M. Rathmann, M. H. Appel, M. R. Henriksen, and J. W. Thomsen, *J. Phys.: Conf. Ser.* **810**, 012002 (2017).
- [57] K. D. Bonin and V. V. Kresin, *Electric-Dipole Polarizabilities of Atoms, Molecules, and Clusters* (World Scientific, Singapore, 1997).
- [58] J. Kaur, D. K. Nandy, B. Arora, and B. K. Sahoo, *Phys. Rev. A* **91**, 012705 (2015).
- [59] U. Safronova, A. Safronova, and P. Beiersdorfer, *J. Phys. B* **39**, 4491 (2006).
- [60] W. R. Johnson, D. R. Plante, and J. Sapirstein, *Adv. At. Mol. Opt. Phys.* **35**, 255 (1995).
- [61] D. Pan, B. Arora, Y. M. Yu, B. K. Sahoo, and J. Chen, *Phys. Rev. A* **102**, 041101(R) (2020).
- [62] B. K. Sahoo, D. K. Nandy, B. P. Das, and Y. Sakemi, *Phys. Rev. A* **91**, 042507 (2015).
- [63] C. Schwartz, *Phys. Rev.* **97**, 380 (1955).
- [64] I. I. Sobelman, in *Atomic Spectra and Radiative Transitions* (Springer, Germany, 1979), pp. 53–88.
- [65] P. Indelicato, *Phys. Rev. Lett.* **77**, 3323 (1996).
- [66] J. W. Farley and W. H. Wing, *Phys. Rev. A* **23**, 2397 (1981).
- [67] Y.-M. Yu and B. K. Sahoo, *Phys. Rev. A* **97**, 041403(R) (2018).
- [68] B. Arora, M. S. Safronova, and C. W. Clark, *Phys. Rev. A* **76**, 064501 (2007).
- [69] B. Arora, D. K. Nandy, and B. K. Sahoo, *Phys. Rev. A* **85**, 012506 (2012).
- [70] C. J. Campbell, A. G. Radnaev, A. Kuzmich, V. A. Dzuba, V. V. Flambaum, and A. Derevianko, *Phys. Rev. Lett.* **108**, 120802 (2012).

- [71] V. A. Dzuba, S. O. Allehabi, V. V. Flambaum, J. Li, and S. Schiller, [Phys. Rev. A **103**, 022822 \(2021\)](#).
- [72] M. Takamoto, F.-L. Hong, R. Higashi, Y. Fujii, M. Imae, and H. Katori, [J. Phys. Soc. Jpn. **75**, 104302 \(2006\)](#).
- [73] S. G. Porsev and M. S. Safronova, [Phys. Rev. A **102**, 012811 \(2020\)](#).
- [74] W. M. Itano, [J. Res. Natl. Inst. Stand. Technol. **105**, 829 \(2000\)](#).
- [75] S. G. Porsev, U. I. Safronova, M. S. Safronova, P. O. Schmidt, A. I. Bondarev, M. G. Kozlov, I. I. Tupitsyn, and C. Cheung, [Phys. Rev. A **102**, 012802 \(2020\)](#).
- [76] B. K. Sahoo, in *Handbook of Relativistic Quantum Chemistry*, edited by W. Liu (Springer, Berlin, 2015), pp. 611–655.
- [77] J. Guéna, R. Li, K. Gibble, S. Bize, and A. Clairon, [Phys. Rev. Lett. **106**, 130801 \(2011\)](#).
- [78] D. J. Wineland, [Rev. Mod. Phys. **85**, 1103 \(2013\)](#).
- [79] J. Zhang, K. Deng, J. Luo, and Z.-H. Lu, [Chin. Phys. Lett. **34**, 050601 \(2017\)](#).
- [80] Y. Huang, B. Zhang, M. Zeng, Y. Hao, Z. Ma, H. Zhang, H. Guan, Z. Chen, M. Wang, and K. Gao, [Phys. Rev. Appl. **17**, 034041 \(2022\)](#).
- [81] W. D. Phillips, [Rev. Mod. Phys. **70**, 721 \(1998\)](#).